metals

MDPI

Article

Effect of Roundness and Surface Roughness of Foundry Sand on the Temperature Change of Sand Cores for Aluminum Casting

Taekyu Ha, Jongmin Kim, Youngki Lee, Byungil Kang and Youngjig Kim *

Department of Advanced Materials Science and Engineering, Sungkyunkwan University, 2066 Seobu-ro, Jangan-gu, Suwon 16419, Republic of Korea; taekyu@skku.edu (T.H.); win95win95@skku.edu (J.K.); galeans@skku.edu (Y.L.); subs39th@skku.edu (B.K.)
* Correspondence: yjk1122@skku.edu

Abstract: Organic binder in sand cores, such as phenol-formaldehyde binder, rapidly decomposes above 550 K, releasing gases including volatile organic compounds (VOCs) and hydrocarbon gases. A rapid temperature rise in the core increases gas evolution during the casting process. The roundness and surface roughness of foundry sand particles influence temperature changes in sand cores. This study investigates how these factors affect temperature change in packed sand beds and cores and the gas porosity at the interface between the core and the A356 Al castings. Temperature changes were measured using three types of sand: angular artificial sand (AAS), natural sand (NS) with different roundness and surface roughness, and polished AAS with a smooth surface. Additionally, the temperature rise in cores was measured with varying proportions of AAS. Packed sand beds and cores with low roundness and rough surface morphology form macro and micro-gaps due to high porosity and surface roughness. These gaps, filled with interstitial gas of low thermal conductivity, hinder heat conduction. Delaying the temperature rise of the core could reduce weight loss from binder decomposition, thereby decreasing gas porosity at the interface between the A356 Al castings and the core. These findings on the effects of roundness and surface roughness on temperature changes in packed sand beds and cores provide methods for reducing gas emission during the casting process.

Keywords: foundry sand; roundness; surface roughness; angular artificial sand; temperature change

Academic Editor: Franc Zupanič

Received: 20 December 2024
Revised: 15 January 2025
Accepted: 16 January 2025
Published: 18 January 2025

Citation: Ha, T.; Kim, J.; Lee, Y.; Kang, B.; Kim, Y. Effect of Roundness and Surface Roughness of Foundry Sand on the Temperature Change of Sand Cores for Aluminum Casting. *Metals* **2025**, *15*, 88. https://doi.org/10.3390/met15010088

1. Introduction

In recent years, the demand for lightweight and multifunctional components in automobile manufacturing has significantly increased due to the need to improve fuel efficiency. This trend has led to an increased use of hollow components, prompting the casting industry to adopt various processes for manufacturing complex shapes, including hollow and thin parts [1,2]. Resin-coated sand (RCS) cores, which utilize an organic binder, are widely used in the casting industry due to their suitability for mass production and the casting of complex forms [3,4]. However, when sand cores come into contact with the high temperatures of molten metal during the casting process, core gas is generated due to the thermal decomposition of organic binders. Gas porosity defects caused by the core gas can be prevented either through venting systems to remove the gas or by using inorganic sand cores. If the core gas is not adequately vented, it can become trapped in the casting before the molten metal solidifies, resulting in gas porosity defects that negatively affect the mechanical properties of the casting [5–8]. To prevent casting defects such as bubble trails caused by core gas, out-gassing is necessary before the gas pressure within the cores

surpasses the pressure of the melts [9,10]. Zhang et al. measured the gas evolution of sand cores with various binders at different temperatures and reported that gas evolution increased significantly at a temperature above 773.15 K [11]. Moreover, Qian et al. investigated the gas evolution characteristics of no-bake, resin-bonded sand at increasing temperatures and observed that gas evolution rose with temperature, and the types of gases emitted varied depending on the type of binder used [12]. Therefore, the temperature of the core significantly affects the extent of gas evolution, as higher temperature increases gas release. This means that suppressing the temperature rise of the core can reduce gas evolution.

The foundry sand used in sand cores is classified into NS and AAS. NS consists mainly of SiO_2, whereas AAS is composed of metal oxides such as Al_2O_3 and MgO along with SiO_2. The manufacturing methods of AAS are categorized into melt-spraying, sintering, and crushing methods. AAS produced by melt spraying and sintering methods is spherical in shape, while sand produced by the crushing method is angular due to the crushing of minerals [13]. The morphology of foundry sand, including its roundness and surface roughness, is critical to controlling temperature changes in packed sand beds and cores. Heat transfer in particulate materials occurs through heat conduction via particle-to-particle contact, macro-gaps formed by the pores of stacked particles, and micro-gaps formed due to surface roughness of the contacting particles [14]. Since interstitial gas has low thermal conductivity, its thermal resistance is higher than that of particle-to-particle contact, resulting in a temperature drop during heat conduction through the interstitial gas. Roundness and surface roughness influence the areas of macro- and micro-gaps in packed sand beds and cores. Consequently, the morphology of foundry sand influences the temperature change in the packed sand beds and cores.

The heat transfer properties of particulate materials, such as sand, have been a subject of interest. Bahrami M. et al. developed a model to predict the effective thermal conductivity of packed beds consisting of rough spheres with uniformed size [15]. Yun T.S. et al. developed a three-dimensional random network model to evaluate thermal conductivity of particulate media. They confirmed that the primary factor controlling thermal conductivity in particulate materials is porosity, which determines the coordination number and mineral fraction [16]. However, the particle shape was limited to circular shape. Fei et al. reported on the relationship between the value of roundness, sphericity, and thermal conductivity of granular materials [17]. Nevertheless, these studies relied on simulation data, which required experimental validation.

Roshankhah S. et al. conducted transient thermal probe measurements to determine the thermal conductivity of a sand–silt mixture. They reported that thermal conductivity follows a linear relationship with the logarithm of effective stress as a consequence of fabric compaction, increased coordination number, contact deformation, and reduced thermal contact resistance [18]. Xiao Y. et al. carried out a series of thermal needle tests on five granular soil mixtures with different proportions of rounded and angular glass particles. They reported that the shape of the particles had less effect on thermal conductivity when the relative density was the same [19]. However, the result of thermal conductivity is controlled by the porosity of the specimen, and when packing the same volume with granular materials, the shape of particles is related to the packing density or void ratio. Beaulieu C. et al. reported that heat transfer through rougher particles is hindered by reduced contact due to surface roughness, as heat transfer in particular materials is influenced by solid microcontact [20]. While their research examined the effects of particle shape and surface roughness in packed beds, it lacked experimental data on sand cores made with foundry sand and binder.

This study investigates how the roundness and surface roughness of foundry sand influence the temperature change of sand cores.

2. Experimental Procedure

2.1. Thermogravimetric Analysis (TGA) for Foundry Sand, RCS, and Phenol-Formaldehyde Binder

TGA was performed to evaluate the weight loss during heating. The specimens included foundry sand, RCS with 1.5 wt% phenol-formaldehyde binder, and binder used for RCS, each of which was analyzed at an amount of approximately 10 mg. TGA was performed from room temperature (RT) to 973.15 K at a heating rate of 10 K/min using a TG/DTA analyzer (TG/DTA 7300, SEICO Instruments Inc., Chiba, Japan). To prevent oxidation, the TGA system was operated in an inert atmosphere with nitrogen gas as purge gas.

2.2. Preparation and Evaluation of the Foundry Sand

NS and AAS, with rounded and angular shapes, respectively, were obtained from WOORI Co., Ltd. in Pyeongtaek, Republic of Korea. NS is a natural aggregate sourced from nature, such as rivers, whereas AAS is manufactured by crushing rocks. The chemical composition of NS and AAS is shown in Table 1. NS consists primarily of SiO_2, whereas the AAS is composed of SiO_2 and various metal oxides. NS consists of >99 wt% SiO_2 with a theoretical thermal conductivity of 0.8 W/m · K, while the AAS contains about 44% metal oxides, which have theoretical thermal conductivities about 10–50 times higher than SiO_2. The characteristics of foundry sands are shown in Table 2. The particle size distribution of NS ranges from 150 to 1200 μm, with the average particle size being 580 μm for NS, and the distribution of AAS ranges from 200 to 1200 μm, with the average particle size being 590 μm for AAS. The pH indicates the impurity contents in foundry sand. The pH values of NS and AAS are 6.4 and 6.3, respectively, resulting in similar impurity levels. The specific gravity, calculated according to AFS 1116-19-S [21], was 2.17 for NS and 2.40 for AAS.

Table 1. Chemical composition of NS and AAS, wt%.

Compound	SiO_2	MgO	Fe_2O_3	CaO	Al_2O_3	K_2O	Na_2O
NS	99.62	0.01	0.01	0.04	0.05	0.01	0.01
AAS	56.00	31.10	7.50	3.40	1.90	0	0

Table 2. Characteristics of NS and AAS.

Parameter	NS	AAS
Manufacture process	Extracted from natural environment	Rock crushing
AFS-GFN	30.9	29.6
Diameter (μm)	580	590
pH	6.4	6.3
Specific gravity	2.17	2.40
Shape	Rounded	Angular or sub rounded

To investigate the effect of particle surface roughness on the temperature change, 1 kg of AAS was processed using rotary ball milling (BML-2, DAIHAN Scientific, Wonju, Republic of Korea) with alumina abrasive at 300 RPM for 100 h. The polished AAS was sieved into various particle size ranges (0.21–0.25 mm, 0.25–0.30 mm, 0.30–0.40 mm, 0.40–0.60 mm, and 0.60–0.80 mm) to match the particle size distribution of the AAS.

The surface morphology of the sand particles was observed using a scanning electron microscope (SEM, S-3000H, HITACHI, Tokyo, Japan). Roundness was measured according to Kuo C.Y. et al. [22]. As shown in Figure 1, the SEM images were preprocessed by filling the sand particles with black. For the average roundness of sand particles, the method described by Cho G.C et al. was referenced [23]. The roundness of 50 sand particles was measured from 8 SEM images observed at 35× magnification, and the average roundness was calculated.

$$R = \frac{4\pi A}{P^2} \quad (1)$$

where P is the perimeter measured from a planar image of particles arranged in the most stable position, and A means a cross-sectional area. R is equal to 1 for a perfectly spherical particle and increases with an increasing particle angle. In addition, the particle size was analyzed using a laser diffraction particle size analyzer (LS 13 320, BECKMAN COULTER, Brea, CA, USA).

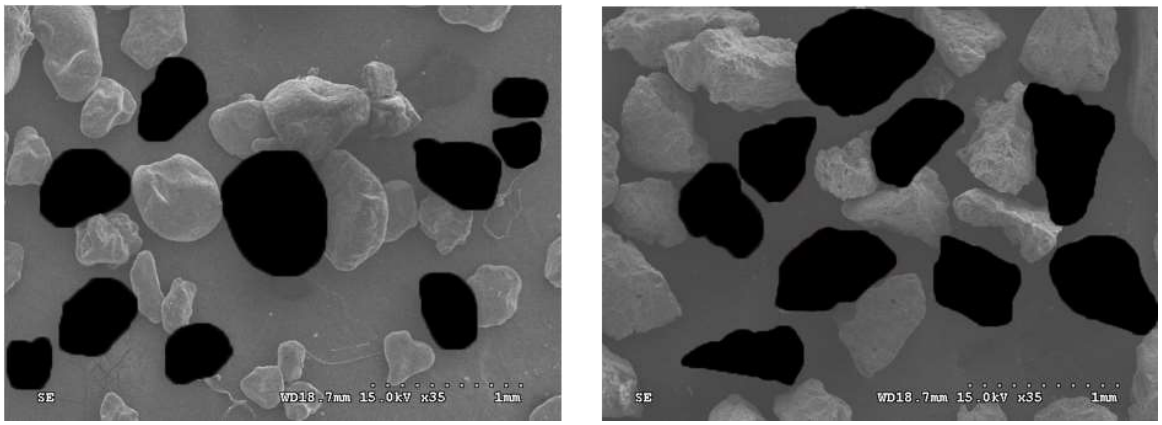

(**a**) (**b**)

Figure 1. SEM image of (**a**) NS, (**b**) AAS at 35× magnifications and method of roundness measurement using image-pro v6.0 software: (**a**) NS, (**b**) AAS.

Surface roughness is described to explain the deviation from a smooth surface of particle. The surface roughness (λ) can be calculated as the ratio of the geometric surface area to the specific surface area [24,25]. The specific surface area of NS, AAS, and polished AAS was measured using Brunauer–Emmett–Teller (BET) analysis (BELSORP-mini II, Microtac BEL, Osaka, Japan).

Surface roughness was calculated using Equation (2) as the ratio of the geometric surface area to the specific surface area.

$$\lambda = \frac{A_{BET}}{A_{GEO}} = \frac{\rho \cdot D \cdot A_{BET}}{6} \quad (2)$$

where A_{BET} (m^2/g) is the specific surface area, calculated through BET isotherm to gas adsorption data. A_{GEO} is a geometric surface area and is calculated by assuming that the particles have regular geometric shapes. ρ $\left(g/cm^3\right)$ is density of particles, and D (μm) is the average particle diameter.

2.3. Temperature Changes in Packed Sand Beds

The effects of the roundness and surface roughness of foundry sand on the temperature changes in packed sand beds were investigated. The comparison between NS and polished AAS, with similar surface roughness, analyzed the effect of roundness, while the comparison between AAS and polished AAS, with similar roundness, focused on the

effect of surface roughness on temperature changes. When a cylindrical insulator (Seoul Industrial Furnace, Kimpo, Republic of Korea) filled with NS, AAS, and polished AAS was heated, axial temperature changes with time were measured at two positions (T_1, T_2). Thermocouples were placed 15 mm apart at the center of the packed sand beds, as shown in Figure 2. The initial temperature (T_i) and the temperature after 30 min (T_f) at each position were measured using a data logger (GL240, GRAPHTEC Corporation, Yokohama, Japan). The weight of foundry sand and its specific gravity are shown in Table 3. Porosity in a packed sand bed is influenced by the roundness of particles. To verify this, NS, AAS, and polished AAS were packed in a cylindrical container, and the porosity of packed sand beds was calculated via Equation (3) based on ASTM C29/C29M [26].

$$\text{Porosity}(\%) = 100[(S \times W) - M]/(S \times W) \quad (3)$$

where S is the specific gravity of foundry sand. W means density of water, 0.997 g/mL at 297.85 K. M is the bulk density of each foundry sand, calculated by dividing the weight of the sand in a cylindrical container by its volume.

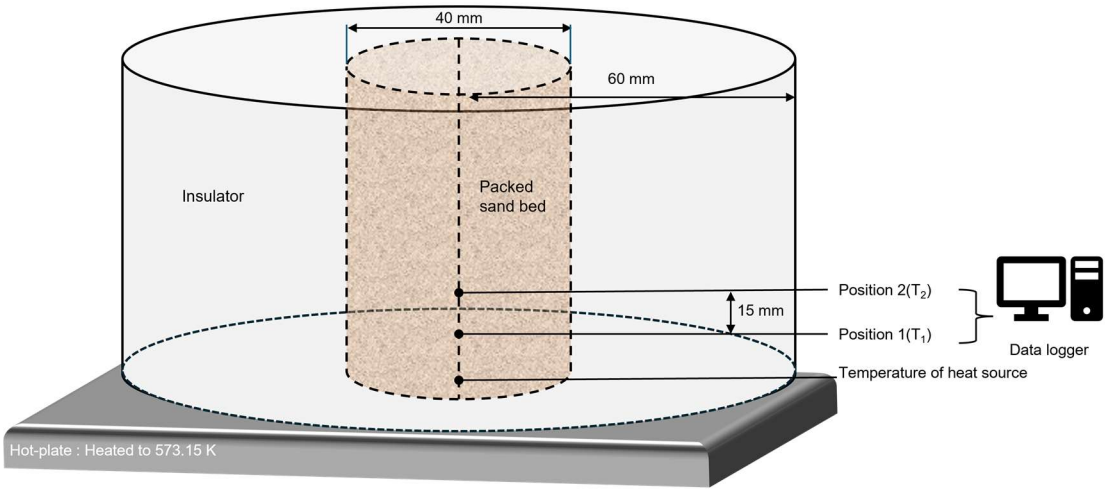

Figure 2. Schematic diagram for measurement of temperature changes in packed sand beds.

Table 3. Weight and specific gravity of foundry sand for temperature change test.

Foundry Sand	Weight (g)	Specific Gravity
NS	218	2.17
AAS	208	2.40
Polished AAS	215	2.38

2.4. Heating and Immersion Test of Sand Cores

The sand cores were manufactured via the shell process for aluminum casting and were cured at 573.15 K for 60 s. NS and AAS were coated with a phenol-formaldehyde binder, with the binder content being 1.5 wt% of the foundry sand weight. The mixed RCS for making sand cores contained resin-coated AAS in ratios of 0%, 10%, 30%, 50%, and 70%, balanced with resin-coated NS. Figure 3 shows the schematic diagram of (a) the heating and (b) immersion test. During the heating test, argon gas was purged into the furnace to prevent oxidation and maintain an inert atmosphere. The sand cores were heated from RT to 673.15 K at a heating rate of 10 K/min.

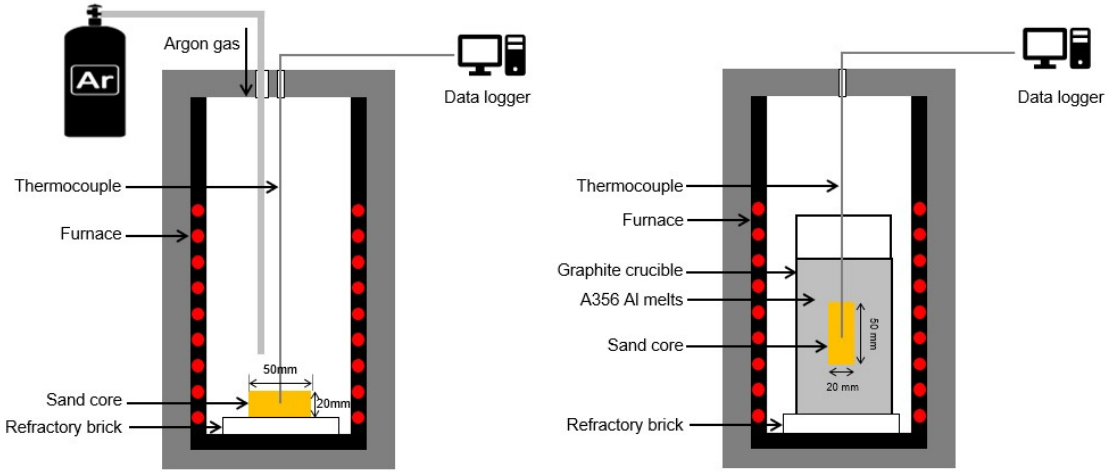

Figure 3. Schematic diagram of apparatus for temperature change in sand core: (**a**) heating test; (**b**) immersion test.

An immersion test was conducted as shown in Figure 3b. The experimental alloy was A356 aluminum, and its chemical composition is shown in Table 4. The sand cores were immersed in 1 kg of A356 Al melts at 973.15 K. Heating and immersion tests were conducted to measure the temperature change at the center of the sand core with time for different ratios of resin-coated AAS.

Table 4. Chemical composition of A356 Al alloy (wt%).

Element	Si	Cu	Mg	Mn	Fe	Al
A356 Al alloy	6.9	0.2	0.4	0.1	0.1	Bal.

2.5. Measurement of Internal Porosity in the Sand Cores

To determine whether the reduced packing density due to the angular particle shape of sand affects porosity, MIP analysis was performed on both the AAS core and NS core using a mercury porosimeter (Autopore IV 9520, Micromeritics instrument Co., Norcross, GA, USA). The size of the test specimens was 5 mm × 5 mm × 5 mm, with the average weight of the NS core being 0.93 g and the AAS core being 0.97 g. Each specimen was preheated at 383.15 K for 1 h to remove moisture. The internal porosity of the sand core was calculated using Equation (4).

$$\text{Porosity}(\%) = \frac{b - a}{b} \times 100 \quad (4)$$

where a is the volume of the specimen, including pores but excluding the voids between particles, calculated by dividing the weight of the specimen by the apparent density. while b is volume of the specimen including pores and the voids between particles, calculated by dividing the weight of the specimen by the bulk density.

2.6. Microstructural Analysis of the Interface Between A356 Al Castings and the Sand Cores

The interfaces between A356 Al castings and the NS core and between A356 Al castings and the AAS core were compared. An A356 Al alloy ingot (2 kg) was held in a graphite crucible and melted in the electric furnace (Seoul Industrial Furnace, Kimpo, Republic of Korea) at 973.15 K. The A356 Al melts were ultrasonically degassed. A rectangular sand core with dimensions of 50 mm × 20 mm × 20 mm was placed inside the stainless-steel

crucible with an inner diameter of 100 mm and a height of 150 mm. The A356 Al melts were poured at 963.15 K into a crucible and solidified under air conditions. During solidification, the temperature of the A356 Al melts at 5 mm above the sand core and the temperature at the center of the sand core were measured. Gas porosity in the approximately 15.7 mm^2 area at the interface between A356 Al castings and core was examined using an optical microscope (DM2700M, Leica microsystems GmbH, Wetzlar, Germany).

3. Results and Discussion

3.1. TGA Results for Foundry Sand, RCS, and Phenol-Formaldehyde Binder

Figure 4a shows the weight loss of foundry sand and RCS with 1.5 wt% binder as a function of temperature. The foundry sand did not exhibit any weight loss during heating. In contrast, the TG curve of RCS showed a single nodal point. Weight loss occurred from 400 K to 670 K, followed by a second phase of significant weight loss between 670 K and 950 K. In the TG curve of the binder shown in Figure 4b, two nodal points were observed. A slight weight loss occurred from 400 K to 550 K, followed by a huge weight loss from 550 K to 670 K. The weight loss is attributed to the thermal decomposition of the phenolic binder into volatile organic compounds (VOCs) or hydrocarbon gases in an inert atmosphere [27–30]. TG curves for RCS and the binder indicate a significant increase in gas evolution between 550 K and 700 K. Therefore, the extent of gas evolution from cores with differing roundness and surface roughness can be explained by the time required to reach 550 K.

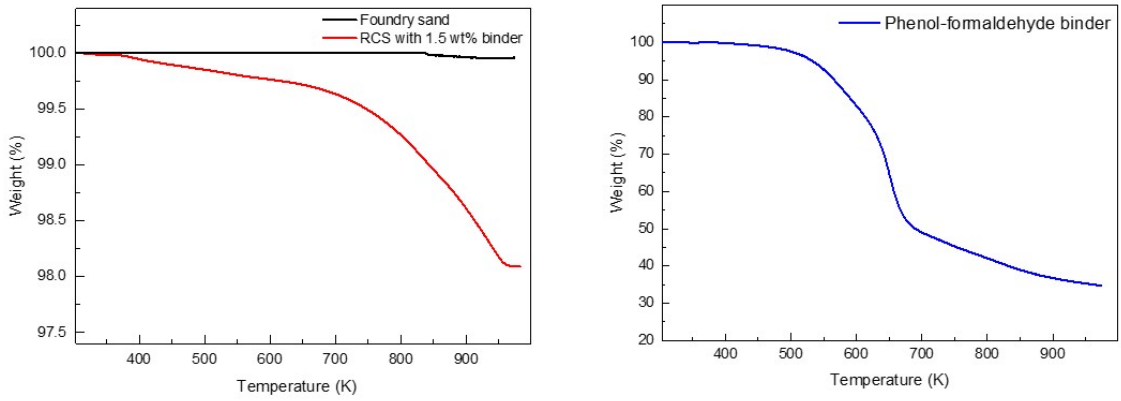

(**a**) (**b**)

Figure 4. Result of TG analysis: (**a**) foundry sand and RCS with 1.5 wt% binder, (**b**) phenol-formaldehyde binder.

3.2. The Influence of Roundness and Surface Roughness on Temperature Changes in Packed Sand Beds

As shown in Figure 5, the surface morphology of AAS and polished AAS indicates that polished AAS has a smoother surface morphology compared to AAS. The particle size distribution of NS, AAS, and polished AAS was in the range of 150 to 1200 µm. The average roundness of NS, which has a rounded shape, was 0.81, while that of AAS, with its angular shape, was 0.45. The roundness of polished AAS, which was polished using alumina, was 0.48, similar to that of AAS.

Table 5 shows the bulk density, specific gravity, and porosity for NS, AAS, and polished AAS in the packed sand bed. The packed NS bed, with a roundness of 0.81, had a porosity of 25%, while the packed AAS bed, with a roundness of 0.45, had a porosity of 39%. The packed polished AAS bed showed porosity of 36% due to its angular shape. This confirms that a lower roundness of foundry sand increases the porosity in the packed sand bed, while surface roughness has negligible effect on the porosity between the particles.

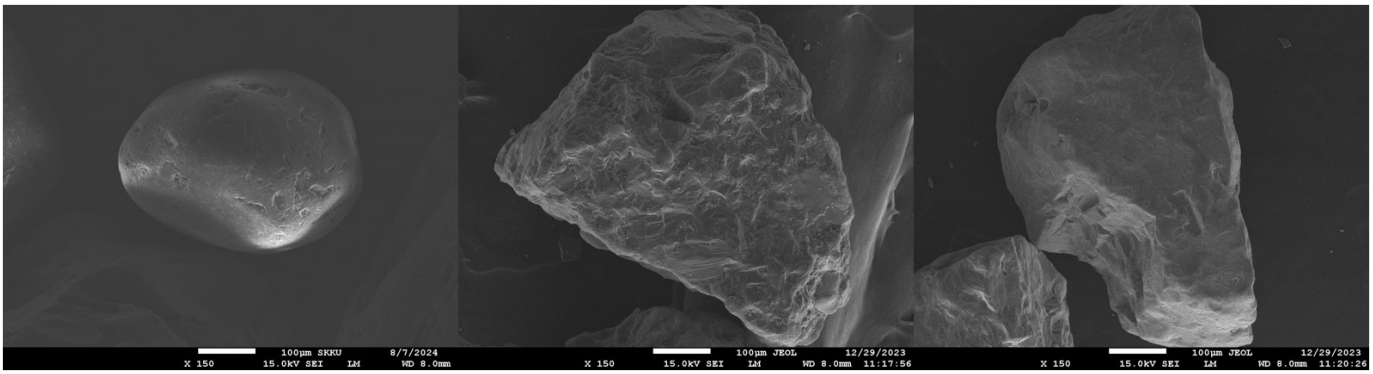

(**a**) (**b**) (**c**)

Figure 5. Morphology of foundry sand at 150× magnifications: (**a**) NS; (**b**) AAS; (**c**) polished AAS.

Table 5. Specific gravity, bulk density, and porosity of different foundry sand in packed sand bed.

Foundry Sand	Specific Gravity	Bulk Density (g/mL)	Porosity (%)
NS	2.17	1.48	25
AAS	2.40	1.63	39
Polished AAS	2.38	1.66	36

For NS, the specific surface area is 0.101 m^2/g with a surface roughness of 21.13, while AAS has a specific surface area of 0.285 m^2/g and a surface roughness of 67.07, approximately three times higher. Polished AAS has a similar specific surface area and surface roughness to NS, at 0.104 m^2/g and 24.27. NS has a rounded shape and smooth surface, AAS has an angular shape and rough surface, and polished AAS has an angular shape and smooth surface. Table 6 shows the roundness and surface roughness of the three types of packed sand beds.

Table 6. Roundness and surface roughness of NS, AAS, and polished AAS.

Type of Packed Sand Beds	Roundness	Surface Roughness
NS	0.81	21.1
AAS	0.45	67.1
Polished AAS	0.48	24.3

The temperature change in packed sand beds was measured to assess the effects of roundness and surface roughness on heat conduction. Figure 6 shows the axial temperature change with time when the packed sand beds (NS, AAS, and polished AAS) were heated for 30 min.

The temperature changes in the NS-packed bed and the polished AAS-packed bed, which have similar surface roughness but different roundness, were compared. NS, with a roundness of 0.81, and polished AAS, with a roundness of 0.48, showed comparable temperature changes and gradients in 30 min. At position 1 (T_1), the temperature of the NS-packed bed increased from 293 K to 474 K, while the polished AAS-packed bed increased from 295 K to 477 K, both with an average temperature gradient of 6.0 K/min in 30 min. At position 2 (T_2), the temperature of the NS-packed bed increased from 293 K to 366 K, and the polished AAS-packed bed increased from 295 K to 374 K, with an average temperature gradient of 2.4 K/min and 2.6 K/min in 30 min, respectively. Despite the higher theoretical thermal conductivity of AAS, which contains approximately 50 wt% metal oxides, the temperature changes were similar due to the lower roundness of AAS.

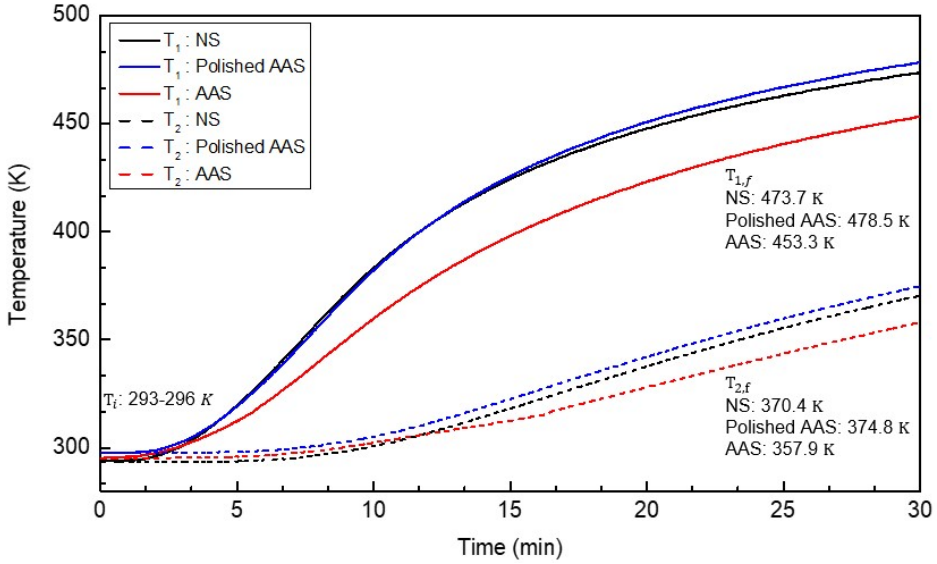

Figure 6. Result of temperature change test in the packed sand beds for NS, AAS, and polished AAS.

The temperature changes of packed sand beds in polished AAS and AAS, which have similar roundness but surface roughness values of 67.07 and 24.27, respectively, were compared. At T_1, the temperature of the polished AAS-packed bed increased from 295 K to 477 K, with an average temperature gradient of 6.0 K/min in 30 min, while the AAS-packed bed increased from 295 K to 453 K with an average temperature gradient of 5.3 K/min in 30 min. At T_2, the temperature of the polished AAS-packed bed increased from 295 K to 374 K with an average temperature gradient of 2.6 K/min in 30 min, whereas the AAS-packed bed increased from 295 K to 357 K with an average temperature gradient of 2.1 K/min in 30 min. The temperature change in the polished AAS-packed bed was 15% higher at $T_{1,f}$, and 23% higher at $T_{2,f}$ compared to the AAS-packed bed. These results can be attributed to the surface roughness of the foundry sand. Although the roundness was similar, the packed sand bed using AAS particles with higher surface roughness showed lower temperature changes during heating compared to polished AAS.

Heat energy in packed sand beds is transferred through radiation, conduction between particle-to-particle contact, and conduction via interstitial gas within macro-gaps and micro-gaps. In most applications where the joint temperature at the particle-to-particle contact is below 873.15 K, radiation can be neglected [31]. Figure 7 shows the schematic of the heat flow in packed sand beds of foundry sand; (a) presents the heat conduction in packed sand bed with high roundness and low surface roughness, while (b) shows the heat conduction in packed sand bed with low roundness and high surface roughness. In schematic diagram (b), the lower roundness results in larger macro-gaps, and the rough surface leads to the formation of micro-gaps between contacting particles. Both macro- and micro-gaps are filled with interstitial gas. Interstitial gas, such as air, has poor thermal conductivity, with air specifically showing a thermal conductivity ranging from 2.623×10^{-2} to 6.763×10^{-2} W/m·K between 300 and 900 K [32]. Due to the higher thermal resistance compared to particle-to-particle contact, heat conduction through interstitial gas results in a significant temperature drop. The results of the temperature change in packed sand beds with different roundness are consistent with those of Rodrigues S.J. et al., who reported that in the region of moderate particle thermal conductivity, the effective thermal conductivity of the bed depends on its porosity and the shape factor [33]. In addition, the results from packed sand beds with varying surface roughness align with those of Bahrami M. et al. [15], who indicated that rough surfaces reduce the contact area between particle surfaces and impede heat transfer. Furthermore, Beaulieu C. [20] also explained that for

particles with high thermal conductivity, heat is mainly transferred through the contact area between the sand particles. The results of this experiment confirmed that roundness and surface roughness have a dominant effect on the heat conduction of foundry sand, in addition to theoretical thermal conductivity.

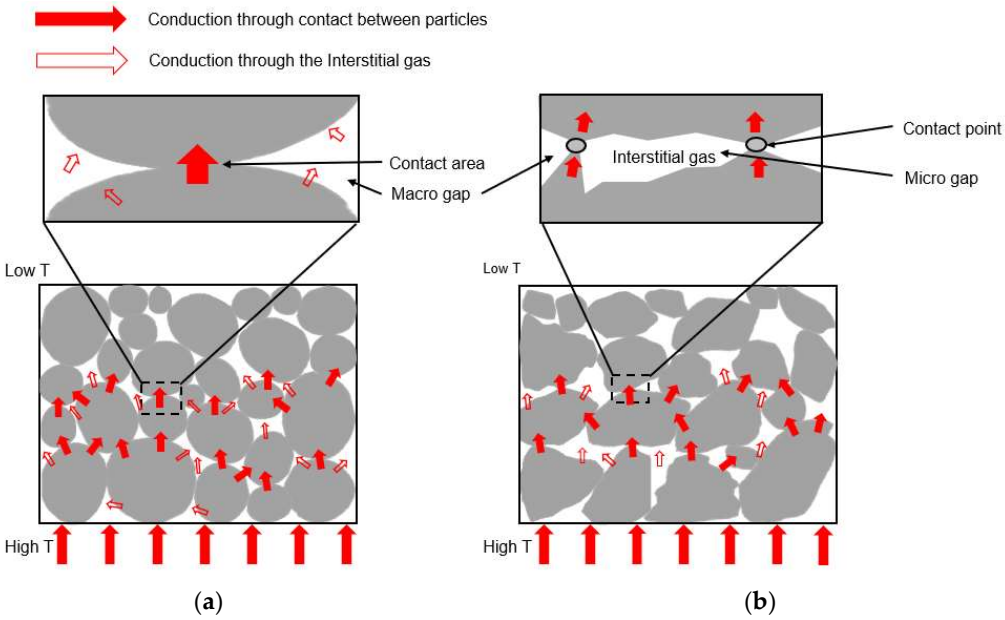

Figure 7. The schematic diagram for heat flow: (**a**) foundry sand with high roundness and smooth surface, (**b**) foundry sand with low roundness and rough surface. Arrows indicate the extent of heat flow through the contact area, macro-gaps, and micro-gaps.

3.3. The Influence of Roundness and Surface Roughness on Temperature Changes in Sand Cores

Heating and immersion tests were conducted on mixed sand cores with different proportions of AAS and NS. During the heating and immersion tests, the volume of sand particles thermally expanded as the core temperature increased. However, this study focused on the time required to reach 550 K when sand cores were heated from RT to 673.15 K at a heating rate of 10 K/min or immersed in A356 Al melts at 973.15 K. According to Svidró J. et al., thermal expansion of silica sand at 550 K is approximately 0.4% [34]. Therefore, the effects of thermal expansion were considered negligible compared to the particle spacing caused by the burnout of binder bridges or the porosity resulting from the roundness of the sand particles.

The results of the heating test of the sand cores according to various resin-coated ratio are presented in Figure 8. The temperature at the center of the sand core without resin-coated AAS (NS core) reached 550 K, the temperature at which the phenolic binder rapidly decomposes and releases core gas, in 25 min. In contrast, the AAS core with a 70% ratio reached 500 K within the same time, resulting in a 10% lower temperature change. The experimental results also showed that the temperature changes became similar when the resin-coated AAS content was 30% or more.

Figure 9 shows the results of the immersion test of the sand core specimens with various ratios of resin-coated AAS contents. Similar to the results of heating test, the temperature changes at the center of the NS core without resin-coated AAS reached 550 K in 22 s when immersed in 973.15 K A356 Al melts. However, the AAS core with a 70% ratio reached only 340 K at the same time, with temperature changes approximately 40% lower. As the ratio of resin-coated AAS content increased, the temperature changes tended to decrease.

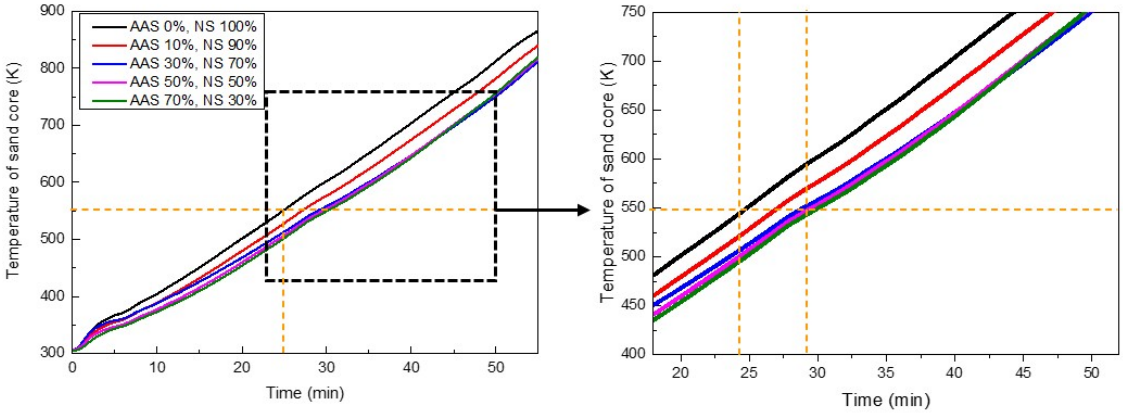

Figure 8. Heating test results of various ratios of AAS cores. The orange dashed lines indicate the time for the NS core and the AAS core with a 70% ratio to reach 550 K

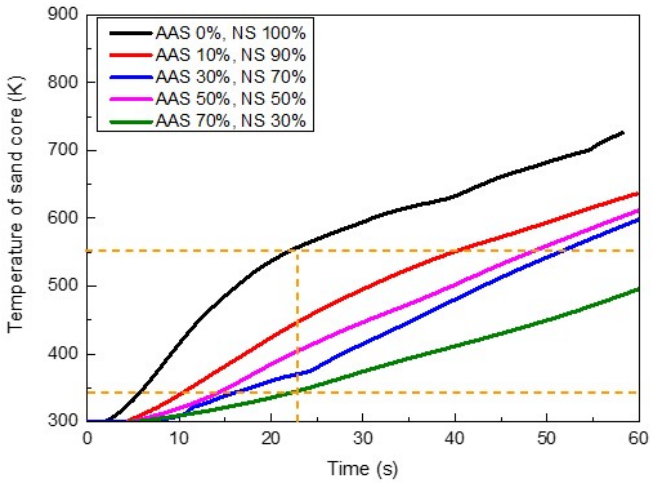

Figure 9. Immersion test result of various ratios of AAS cores. The orange dashed lines indicate the temperature of the NS core and AAS core with a 70% after 22 seconds of immersion in 973.15 K A356 Al melts.

These results of the heating and immersion tests showed a slower temperature change in sand cores with the addition of AAS. To explain this behavior, mercury intrusion porosimetry (MIP) analysis was performed to measure the pore distribution and porosity of the NS and AAS cores. Figure 10 shows the MIP results of the NS core and AAS core specimen. The solid line represents the cumulative intrusion, indicating the total pore volume. The dashed lines represent the log differential intrusion, indicating the changes in mercury intrusion, which reflects the pore distribution. The total pore volume of the AAS core was higher than that of the NS core, Additionally, the pore distribution showed that both the NS and AAS cores had the highest concentration of pores with a diameter of 100 μm, due to the similar size of the sand particles and the binder bridges between sand particles. However, the AAS core showed a greater number of pores larger than 600 μm, which is attributed to the lower roundness of AAS. Table 7 shows the mean pore diameter, apparent density, bulk density, and porosity of the NS core and AAS core.

Figure 11 shows the binder bridge areas among sand particles in the NS and AAS cores. The porosity of the NS core was 8% lower than that of the AAS core, indicating a reduced binder bridge area among the sand particles. The low roundness of foundry sand leads to an increase in porosity, forming macro-gaps among the sand particles. Macro-gaps cause a reduction in the coordination number and contact area, which are parameters for heat conduction in granular materials. The results of this study experimentally verified that

lower roundness and higher surface roughness of sand particles impede heat conduction, consistent with previous studies [14–20,33]. While previous studies conducted experiments on the packed beds, this study confirms that the roundness of the foundry sand also affects the porosity of sand cores with binder, hindering temperature changes.

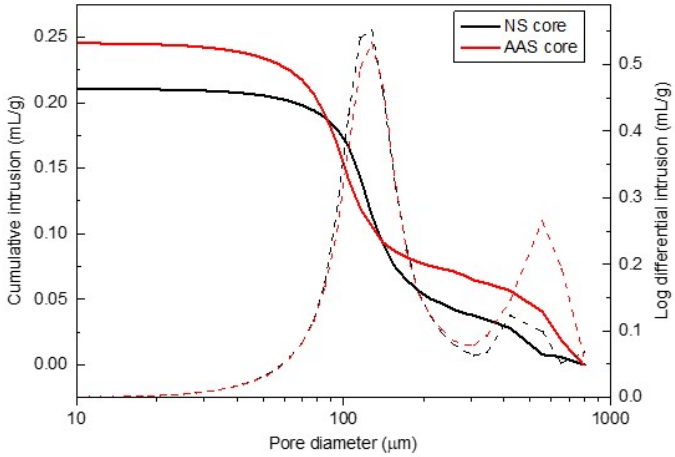

Figure 10. Cumulative intrusion and pore diameter distribution of NS and AAS cores.

Table 7. Mean pore diameter, apparent density, bulk density, and porosity of NS core and AAS core.

Sand Core	Mean Pore Diameter (μm)	Apparent Density (g/mL)	Bulk Density (g/mL)	Porosity (%)
NS core	112	2.54	1.65	35
AAS core	127	3.00	1.73	42

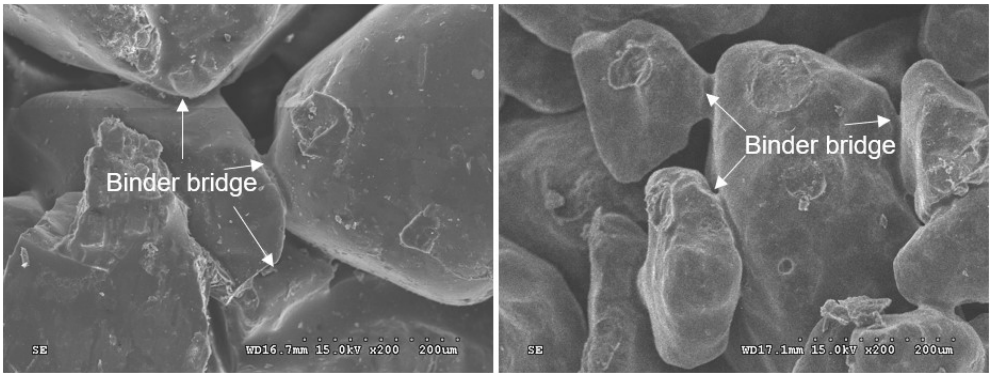

(**a**) NS core (**b**) AAS core

Figure 11. Morphology of sand cores at 200× magnifications.

Figure 12 shows the cooling curves of A356 Al alloy during solidification, measured 5 mm above the core and at the center of the cores. The black and red dashed lines indicate the time to reach 550 K, the temperature at which gas is significantly released from the core. The NS core reached 550 K in 66 s, while the AAS core took 88 s. Gas porosity in the A356 Al alloy is caused by core gas trapped within the castings during the phase transformation from the mushy zone to solid phase [35]. The NS core exhibited a faster temperature rise compared to the AAS core. This suggests a difference in gas porosity at the interface between the core and the A356 Al alloy.

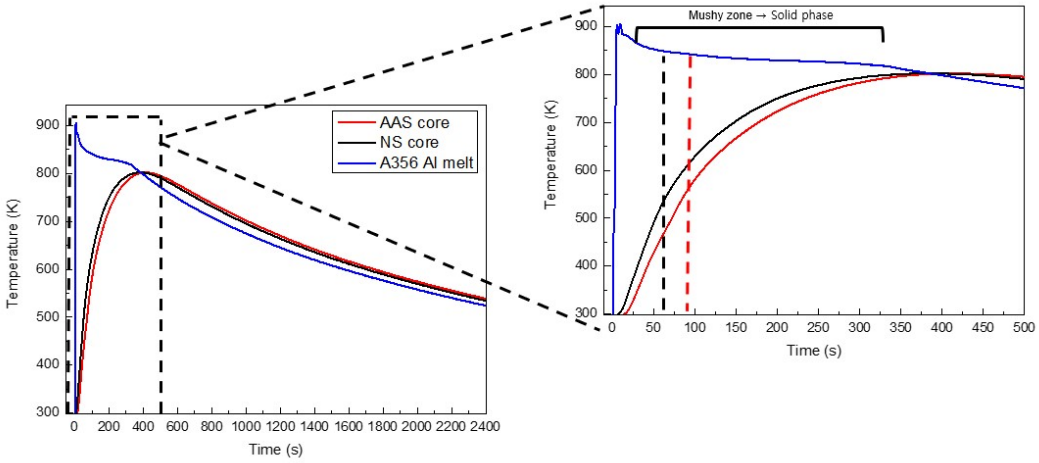

Figure 12. The cooling curves during the solidification of A356 Al alloy measured 5 mm above the sand core and at the center of the cores. The black and red lines indicate the time to reach 550 K for the NS core and AAS core, respectively.

Figure 13 shows the typical microstructure of the interface area, approximately 15.7 mm^2, between the core and A356 Al alloy. Gas porosity was observed at the interface for both the NS core and AAS core. However, the gas porosity is higher in NS core specimens, with a porosity of 1.1%, while the AAS core resulted in smaller pores, with a porosity of 0.3%. The macro-gaps between particles due to the low roundness of AAS and the micro-gaps caused by their rough surfaces reduce heat conduction when in contact with the A356 Al melts during casting process, leading to reduced gas porosity.

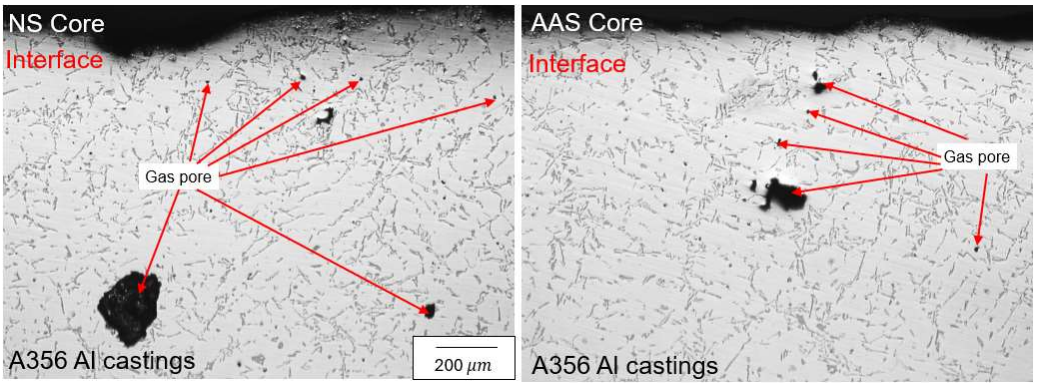

(**a**) (**b**)

Figure 13. The typical microstructure at the interface between the sand core and A356 Al castings: (**a**) NS core and A356 Al castings, (**b**) AAS core and A356 Al castings.

4. Conclusions

This study investigated how the roundness and surface roughness of foundry sand influence the temperature change of packed sand beds and sand cores.

As the temperature increases, the weight of RCS and the binder decreases, with a significant weight loss occurring between 550 K and 700 K. The weight loss of RCS and binder is attributed to the thermal decomposition of the phenolic binder into VOCs and hydrocarbon gases. Therefore, the temperature changes with time of the cores with different roundness and surface roughness should be compared based on the time required to reach 550 K.

(1) The roundness of the foundry sand influences the porosity of the packed sand beds and sand cores. The pores formed by stacked particles, referred to as macro-gaps, are filled with interstitial gas. Interstitial gas within macro-gaps has low thermal conductivity, which hinders heat conduction and slows temperature changes in the packed sand beds and sand cores. The packed NS bed with a roundness 0.81 had a porosity of 25%, whereas the packed polished AAS bed with a roundness of 0.48 had a porosity of 36%. Additionally, the porosity of NS core was 8% lower than that of the AAS core. These results indicate that as the roundness of foundry sand decreases, the porosity of the packed sand beds and cores increases.

(2) Surface roughness affects the temperature change in packed sand beds and sand cores. Micro-gaps, which are pores formed by the contact of particles with rough surfaces, are filled with interstitial gas that slows down temperature changes. The results of the temperature change test indicate that the AAS bed and polished AAS bed have similar roundness, but the surface roughness of the AAS bed is approximately three times lower. As a result of its lower surface roughness, the polished AAS bed shows 15% and 23% higher temperature changes at $T_{1,f}$ and $T_{2,f}$, respectively, compared to the AAS bed.

(3) The increased macro-gaps due to the low roundness and the micro-gaps caused by the rough surface of the AAS core slow temperature changes in the sand core during contact with A356 Al melts in casting, consequently reducing gas porosity. The gas porosity at the interface between the A356 Al castings and the AAS core (gas porosity: 0.3%) was reduced by approximately a factor of 4 compared to that at the interface with the NS core (gas porosity: 1.1%).

Author Contributions: Conceptualization, T.H., J.K., Y.L., B.K. and Y.K.; methodology, T.H.; validation, J.K. and B.K.; data curation, T.H. and Y.L.; writing—original draft preparation, T.H., J.K., Y.L. and B.K.; writing—review and editing, T.H. and Y.K.; supervision, T.H. and Y.K.; formal analysis, B.K. and J.K.; investigation, T.H., Y.L. and J.K All authors have read and agreed to the published version of the manuscript.

Funding: This work was supported by the Technology Innovation Program (00154970, Development of entry-level inorganic binder and exclusive casting process to realize carbon neutral) funded by the Ministry of Trade Industry & Energy (MOTIE, Korea).

Data Availability Statement: The original contributions presented in the study are included in the article; further inquiries can be directed to the corresponding author.

Conflicts of Interest: The authors declare no conflicts of interest.

References

1. Thies, C.; Hüls, C.; Kieckhäfer, K.; Wansart, J.; Spengler, T.S. Project portfolio planning under CO_2 fleet emission restrictions in the automotive industry. *J. Ind. Ecol.* **2022**, *26*, 937–951. [CrossRef]
2. Yu, W.; He, H.; Cheng, N.; Gan, B.; Li, X. Preparation and experiments for a novel kind of foundry core bind-er made from modified potato starch. *Mater. Des.* **2009**, *30*, 210–213. [CrossRef]
3. McIntyre, S. Shell molding and shell coremaking. In *Casting, Editing ASM Handbook Committee*; ASM International: Geauga County, OH, USA, 2008; Volume 15, pp. 598–616.
4. Budavári, I.; Varga, L. The Effect of coremaking parameters on the thermal distortion behavior of resin-coated Sand. *Mater. Sci. Eng.* **2022**, *45*, 37–49.
5. Bargaoui, H.; Azzouz, F.; Thibault, D.; Cailletaud, G. Thermomechanical behavior of resin bonded foundry sand cores during casting. *J. Mater. Process. Technol.* **2017**, *246*, 30–41. [CrossRef]
6. Fortini, A.; Merlin, M.; Raminella, G. A comparative analysis on organic and inorganic core binders for a gravity diecasting Al alloy component. *Int. J. Met.* **2022**, *16*, 674–688. [CrossRef]

7. Naro, R.L.; Pelfrey, R.L. Gas evolution of synthetic core binders: Relationship to casting blowhole defects. *AFS Trans.* **1983**, *91*, 365–376.
8. Starobin, A.; Hirt, C.W.; Goettsch, D. A model for binder gas generation and transport in sand cores and molds. In Proceedings of the Modeling of Casting, Welding and Advanced Solidification Processes XII (TMS 2009), Vancouver, Canada, 7–14 June 2009; pp. 345–352.
9. Kim, H.J. Systematical Approach for Vent Design of Core Out-Gassing Through Development of an Inventive Evaluation Device. *Inter. J. Met.* **2019**, *13*, 890–896. [CrossRef]
10. Monroe, R. Porosity in castings. *AFS Trans.* **2005**, *113*, 519–546. [CrossRef]
11. Zhang, B.; Garro, M.; Chautard, D.; Tagliano, C. Gas evolution from resin-bonded sand cores prepared by various processes. *Metall. Sci. Technol.* **2002**, *20*, 27–32.
12. Qian, X.W.; Wan, P.; Yin, Y.J.; Qi, Y.Y.; Ji, X.Y.; Shen, X.u.; Li, Y.C.; Zhou, J.X. Gas evolution characteristics of three kinds of no-bake resin-bonded sands for foundry in production. *China Foundry* **2022**, *19*, 140–148. [CrossRef]
13. Kurokawa, Y.; Huanf, Z. Particles strength improvement of artificial sand by heat treatment. *J. Jpn. Fou. Eng. Soc.* **2022**, *94*, 254–258.
14. Rouhani, M.; Bahrami, M. Effective thermal conductivity of packed bed adsorbers: Part 2-Theoretical model. *Int. J. Heat Mass Tranf.* **2018**, *123*, 1212–1220. [CrossRef]
15. Bahrami, M.; Yovanovich, M.M.; Culham, J.R. Effective thermal conductivity of rough spherical packed beds. *Int. J. Heat Mass Tranf.* **2006**, *49*, 3691–3701. [CrossRef]
16. Yun, T.S.; Evans, T.M. Three-dimensional random network model for thermal conductivity in particulate materials. *Comput. Geotech.* **2010**, *37*, 991–998. [CrossRef]
17. Fei, W.; Narsilio, G.A.; Disfani, M.M. Impact of three-dimensional sphericity and roundness on heat transfer in granular materials. *Powder Technol.* **2019**, *355*, 770–781. [CrossRef]
18. Roshankhah, S.; Garcia, A.V.; Santamarina, J.C. Thermal conductivity of sand-silt mixtures. *J. Geotech. Geoenviron. Eng.* **2021**, *147*, 06020031. [CrossRef]
19. Xiao, Y.; Ma, G.; Nan, B.; McCartney, J.S. Thermal conductivity of granular soil mixtures with contrasting particle shapes. *J. Geotech. Geoenviron. Eng.* **2020**, *146*, 06020004. [CrossRef]
20. Beaulieu, C.; Vidal, D.; Yari, B.; Chaouki, J.; Bertrand, F. Impact of surface roughness on heat transfer through spherical particles packed beds. *Chem. Eng. Sci.* **2021**, *231*, 116256. [CrossRef]
21. Thomas, S. *Mold&Core Test Handbook*, 5th ed.; American Foundry Society: Schaumburg, IL, USA, 2019; pp. 35–36.
22. Kuo, C.Y.; Rolling, R.S.; Lynch, L.N. Morphological study of coarse aggregates using image analysis. *J. Mater. Civ. Eng.* **1998**, *10*, 135–142. [CrossRef]
23. Cho, G.C.; Dodds, J.; Santamarina, J.C. Particle shape effects on packing density, stiffness, and strength: Natural and crushed sands. *J. Geotech. Geoenviron. Eng.* **2006**, *132*, 591–602. [CrossRef]
24. Hodson, M.E. Micropore surface area variation with grain size in unweathered alkali feldspars: Implications for surface roughness and dissolution studies. *Geochim. Cosmochim. Acta* **1998**, *62*, 3429–3435. [CrossRef]
25. Rezai, B.; Rahimi, M.; Aslani, M.R.; Eslamian, A.; Dehghani, F. Relationship between surface roughness of minerals and their flotation kinetics. In Proceedings of the XI international seminar on Mineral Processing Technology, Jamshedpur, India, 15–17 December 2010; pp. 232–238.
26. *C29/C29M-07*; Standard Test Method for Bulk Density and Voids in Aggregate. ASTM: West Conshohocken, PA, USA, 2007.
27. González, R.; Colás, R.; Velasco, A.; Valtierra, S. Characteristics of phenolic-urethane cold box sand cores for aluminum casting. *Int. J. Metalcast.* **2011**, *5*, 41–48. [CrossRef]
28. Samuels, G.; Beckermann, C. Measurement of gas evolution from PUNB bonded sand as a function of temperature. *Int. J. Metalcast.* **2012**, *6*, 23–40. [CrossRef]
29. Samociuk, B.; Medyński, D.; Nowak, D.; Kawa-Rygielska, J.; Świechowski, K.; Gasiński, A.; Janus, A. The use of barley malt as a binder in molding Sand Technology. *Materials* **2022**, *15*, 3375. [CrossRef] [PubMed]
30. Bryant, N.C.; O'Dell, J.L.; Kowalsky, J.I.; Thiel, G.R. Real-time measurement of mold and core quality in chemically bonded sands. *Int. J. Met.* **2024**, *18*, 14–22. [CrossRef]
31. Yovanovich, M.M.; Marotta, E.E.; Bejan, A.; Kraus, A.D. Thermal spreading and contact resistances. In *Heat Transfer Handbook 1*; John Wiley & Sons, Ltd.: Chichester, UK, 2003; pp. 261–394.
32. Kadoya, K.; Matsunaga, N.; Nagashima, A. Viscosity and thermal conductivity of dry air in the gaseous phase. *J. Phys. Chem. Ref. Data* **1985**, *14*, 947–970. [CrossRef]
33. Rodrigues, S.J.; Vorhauer-Huget, N.; Tsotsas, E. Prediction of effective thermal conductivity of packed beds of polyhedral particles. *Powder Technol.* **2023**, *430*, 118997. [CrossRef]

34. Svidró, J.; Diószegi, A.; Svidró, J.T. The origin of thermal expansion differences in various size fractions of silica sand. *Int. J. Cast Met. Res.* **2020**, *33*, 242–249. [CrossRef]
35. Wang, X.; Wu, Q.; Huang, Y.; Li, N.; Wu, X.; Chen, X.; Kang, J. Study on the Gas Release of 3D-Printed Furan Resin Sand Core during the Casting Process. *Materials* **2023**, *16*, 4152. [CrossRef] [PubMed]